British Journal of Multidisciplinary and Advanced Studies5(4),14-32, 2024

Mathematics, Statistics, Quantitative and Operations Research,

Print ISSN: 2517-276X

Online ISSN: 2517-2778

https://bjmas.org/index.php/bjmas/index

Published by the European Centre for Research Training and Development UK

Mathematical Modelling of the Thermosolutal Effect on Blood Flow through a Micro-Channel in the Presence of a Magnetic Field

J. K. Butter [1], K. W. Bunonyo [2*], and I. C. Eli [3].

[1, 2, 3] Department of Mathematics and Statistics, Federal University Otuoke, Ogbia, Bayelsa State, Nigeria

[2] Mathematical Modelling and Data Analytics Research Group (MMDARG)

wilcoxkb@fuotuoke.edu.ng

doi: https://doi.org/10.37745/bjmas.2022.04161 Published August 22, 2024

Citation: Butter J. K., Bunonyo K. W., and Eli I. C. (2024) Mathematical Modelling of the Thermosolutal Effect on Blood Flow through a Micro-Channel in the Presence of a Magnetic Field, *British Journal of Multidisciplinary and Advanced Studies*, 5(4),14-32, 2024

Abstract: *Substances such as mass concentrations in the blood cause circulation challenges. Blood is a substance made up of 55% plasma and 45% hemoglobin, which flows through the blood vessels and is aided by the heart in pumping to all organs and other tissues and cells in the human body. Mathematical modelling plays an important role in understanding the blood circulation problem in the human body, and it helps transform the real-life cardiovascular problem into a system of mathematical equations. In this research, we transformed the real-life cardiovascular problem of the heat effect on mass concentration and blood flow through blood vessels into a system of partial differential equations representing blood momentum, energy, and mass concentration equations after modifying the Navier-Stoke equation. The models are scaled from dimensional to dimensionless using specific scaling parameters. The scaled dimensionless equations were further perturbed and reduced to a system of ordinary differential equations, and the system of ODEs was solved using the Laplace method, where mathematical models representing blood velocity profiles, temperature profiles, and mass concentration profiles were obtained. A numerical simulation was performed using Wolfram Mathematica, version 12, where the effect of the pertinent parameters on the flow profiles was investigated and the results were presented graphically. The variation of the pertinent parameters such as the Grashof number, solutal Grashof number, Prandtl number, Soret number, Schmidt number, Darcy number, and magnetic field affect the flow profile such that the increase in Grashof number and solutal Grashof number causes the blood velocity to increase substantially at the centre of the vessel before decreasing to zero as the wall boundary layer increases, while the increase in Prandtl number and Soret number increases the blood temperature and velocity.*

Keywords*:* mathematical modelling, thermosolutal, blood, flow, magnetic, field, micro-channel

British Journal of Multidisciplinary and Advanced Studies5(4),14-32, 2024
Mathematics, Statistics, Quantitative and Operations Research,
Print ISSN: 2517-276X
Online ISSN: 2517-2778
https://bjmas.org/index.php/bjmas/index
Published by the European Centre for Research Training and Development UK

Nomenclature

w^*, u^* Dimensional blood velocity in different directions
x^*, r^* Dimensional axial and radial distances
P Dimensionless blood pressure
ρ_b Blood density
μ_b Blood viscosity
$\sum F = F_b + F_m$ Sum of forces acting on the fluid in circulation
T^* Dimensional blood temperature
T_∞ Far field temperature of blood
c_{bp} Blood specific heat capacity
ω Oscillatory frequency
Da Darcy number
ϕ Dimensionless Mass concentration profile
D_0 Diffusivity of the mass concentration
D_T Diffusivity due to temperature
C^* Dimensional mass concentration
C_∞ Far field mass concentration
t Dimensionless time
B Magnetic induction
k^* Porosity
B_0 Magnetic field intensity
M Magnetic field
θ Dimensionless temperature
k_{Tb} Blood thermal conductivity
k_0 Chemical Reactant
Pr Prandtl number
Gr Grashof number
Gc Solutal Grashof number
t Dimensionless Time
Rd Chemical reaction parameter
g Acceleration due to gravity
β_T Volumetric temperature expansion rate
β_C Volumetric concentration expansion rate

British Journal of Multidisciplinary and Advanced Studies5(4),14-32, 2024

Mathematics, Statistics, Quantitative and Operations Research,

Print ISSN: 2517-276X

Online ISSN: 2517-2778

https://bjmas.org/index.php/bjmas/index

Published by the European Centre for Research Training and Development UK

INTRODUCTION

Blood circulation is a continuous loop that delivers oxygen and nutrients to cells while removing waste Athani et al. (2022). The heart pumps oxygenated blood through arteries, which branch into tiny capillaries for exchange. Deoxygenated blood travels through veins back to the heart for re-oxygenation in the lungs Bunonyo & Ebiwareme (2022). Blood vessel narrowing, called stenosis makes it much harder for blood to flow properly. This disrupts blood circulation and heart function. Plaque buildup, a combination of cholesterol and cells, causes the narrowing. The narrower the vessel, the less oxygen-rich blood can get through, raising the risk of heart failure Kubugha & Amos (2022). This narrowing doesn't just affect the amount of blood flow; it also changes the pressure and speed of blood flow throughout the vessel Yusuf *et al.* (2016). Bunonyo and Ebiwareme (2024) investigated the two-dimensional magneto-hydrodynamics laminar flow of a Sisko nanofluid over a nonlinear stretching sheet in a porous medium, considering chemical reactions, the nonlinear Rosseland approximation, and an internal heat source-based on concentration. Yadav and Roshan (2024) investigated the electromagnet hydrodynamic peristaltic flow of blood through the annulus between two concentric circular tubes, aiming to advance peristaltic endoscope technology. Sharma *et al.* (2023) presented a Magneto-hydrodynamics haemodynamics hybrid nanofluid flow through an inclined stenotic artery. Kumawat *et al.* (2021) presented a mathematical analysis of two-phase blood flow through a stenosed curved artery with haematocrit and temperature-dependent viscosity. Shah *et al.* (2021) discussed the effects of pulsatile pressure gradient in the presence of a transverse magnetic field on unsteady blood flow through an inclined tapered cylindrical tube of porous medium. Selvi *et al.* (2021) proposed a theoretical model to investigate the coupled effects of thermal radiation and electromagnetic field on the blood flow in a stenosed tapered artery. Fahim et al. (2024) presented a computational analysis of a Pulsatile pressure-driven non-Newtonian blood flow through a porous stenotic artery using the Navier-Stokes equations and the Carreau fluid model to represent blood rheology. Mamun *et al.* (2020) looked into the influence of a magnetic field on blood flow via a stenotic artery. Ferro-fluids were employed for a variety of purposes, including magnetic separation, anticancer medication delivery, and micro-valves. The research conducted by Priyadharsini (2023) focuses on the mathematical modeling and analysis of the impact of thermoregulation on blood viscosity under magnetic and thermal radiation effects in a porous, stretching blood capillary. The investigation conducted by Hosseinzadeh *et al.* (2022) focused on the study of non-Newtonian blood fluid flow containing nanoparticles within a vessel with a porous wall, in the presence of a magnetic field. Verma & Parihar (2010) developed a mathematical model of blood flow through a tapered artery with mild stenosis and haematocrit. However, the Verma and Parihar research couldn't go further in investigating the effect of the heat on the velocity profile and Bunonyo others didn't study further on the effect of heat on mass concentration and the mass concentration on blood flow profile, which this study aims to achieve.

British Journal of Multidisciplinary and Advanced Studies5(4),14-32, 2024
Mathematics, Statistics, Quantitative and Operations Research,
Print ISSN: 2517-276X
Online ISSN: 2517-2778
https://bjmas.org/index.php/bjmas/index
Published by the European Centre for Research Training and Development UK

Mathematical Formulation

Before we begin developing a system of mathematical models representing the thermosolutal effect on blood flow through a microchannel, consider the following realistic assumptions: The flow is axial; the tangential velocity is assumed to be zero; the fluid is blood, incompressible, and viscous; the viscosity is constant throughout the fluid medium; the flow could be driven by the thermosolutal effect; there is no electrical conductivity in the system; we considered the effect of an external magnetic field; and the blood vessel is porous; the flow obeys the no-slip condition. The mathematical model system is presented based on the assumptions made above and previous research by Bunonyo et al. (2018), Bunonyo and Amos (2023), Hanvey & Bunonyo (2022), and Verma and Parihar (2010).

Current density

The current density with zero electrical conductivity can be stated mathematically as:

$$\vec{J} = \sigma\left(\vec{w} \times \vec{B}\right) \tag{1}$$

Electromagnetic force

The electromagnetic force is the cross product of current density and magnetic field and it can be stated as:

$$\vec{F}_m = \vec{J} \times \vec{B} = -\sigma B_0^2 w^* \tag{2}$$

The force acting along the axial direction:

$$F_x = g\beta_T\left(T^* - T_\infty\right) + g\beta_C\left(C^* - C_\infty\right) \tag{3}$$

The sum of body forces affected blood flow can be stated mathematically as:

$$\sum F = F_m + F_x = -\sigma B_0^2 w^* + g\beta_T\left(T^* - T_\infty\right) + g\beta_C\left(C^* - C_\infty\right) \tag{4}$$

Darcy's law can be stated mathematically as:

$$\left.\frac{\partial P^*}{\partial x^*} = -\frac{\mu_b w^*}{k^*}\right\} \tag{5}$$

Continuity Equation

Following the aforementioned assumptions, the continuity equation can be reduced to:

$$\frac{\partial w^*}{\partial x^*} = 0 \tag{6}$$

Momentum Equation

$$\rho_b \frac{\partial w^*}{\partial t} = \sum F + \frac{\partial P^*}{\partial x^*} + \mu_b\left(\frac{\partial^2 w^*}{\partial r^{*2}} + \frac{1}{r^*}\frac{\partial w^*}{\partial r^*}\right) \tag{7}$$

Momentum Equation according to Verma and Parihar (2010):

$$\rho_b \frac{\partial w^*}{\partial t} = \frac{\partial P^*}{\partial x^*} + \mu_b\left(\frac{\partial^2 w^*}{\partial r^{*2}} + \frac{1}{r^*}\frac{\partial w^*}{\partial r^*}\right) \tag{8}$$

Substituting equations (4) and (5) into equation (7), the momentum equation with the body forces affecting the fluid flow becomes:

Momentum Equation with body the forces

$$\rho_b \frac{\partial w^*}{\partial t} = \mu_b \left(\frac{\partial^2 w^*}{\partial r^{*2}} + \frac{1}{r^*} \frac{\partial w^*}{\partial r^*} \right) - \sigma B_0^2 w^* - \frac{\mu_b w^*}{k^*} + \rho_b g \beta_T \left(T^* - T_\infty \right) + \rho_b g \beta_C \left(C^* - C_\infty \right) \tag{9}$$

Energy Equation

Following Bunonyo *et al*. (2018), the energy equation is:

$$\rho_b c_{bp} \frac{\partial T^*}{\partial t^*} = k_{Tb} \left(\frac{\partial^2 T^*}{\partial r^{*2}} + \frac{1}{r^*} \frac{\partial T^*}{\partial r^*} \right) \tag{10}$$

Mass Concentration Equation

Following Bunonyo *et al*. (2021), the mass concentration equation is

$$\frac{\partial C^*}{\partial t^*} = D_0 \left(\frac{\partial^2 C^*}{\partial r^{*2}} + \frac{1}{r^*} \frac{\partial C^*}{\partial r^*} \right) - k_0 \left(C^* - C_\infty \right) + \frac{D_T k_{Tb}}{T_m} \left(\frac{\partial^2 T^*}{\partial r^{*2}} + \frac{1}{r^*} \frac{\partial T^*}{\partial r^*} \right) \tag{11}$$

The corresponding boundary conditions are:

$$\left.\begin{array}{l} w^* = 0, T^* = T_w, C^* = C_w \quad \text{at } r^* = R \\ w^* \neq 0, T^* \neq T_w, C^* \neq C_w \quad \text{at } r^* = 0 \end{array}\right\} \tag{12}$$

Dimensionless Quantities

$$\left.\begin{array}{l} x^* = x\lambda, r^* = rR_0, \upsilon_b = \dfrac{\mu_b}{\rho_b} w^* = \dfrac{w\upsilon_b}{R_0}, t^* = \dfrac{R_0^2 t}{\upsilon_b}, P = \dfrac{R_0^3 P^*}{\upsilon_b \mu_b \lambda}, Rd = \dfrac{k_0 R_0^2}{D_0}, \mu_b = \rho_b \upsilon_b \\ \dfrac{\partial P^*}{\partial x^*} = \rho_\infty \vec{g}_x, Gr = \dfrac{\vec{g}_x \beta_T \left(T_w - T_\infty \right) R_0^3}{\upsilon_b^2}, Sr = \dfrac{D_T k_{Tb} \left(T_w - T_\infty \right)}{D_0 T_m \left(C_w - C_\infty \right)} Gc = \dfrac{\vec{g}_x \beta_C \left(C_w - C_\infty \right) R_0^3}{\upsilon_b^2}, \\ \theta = \dfrac{T^* - T_\infty}{T_w - T_\infty}, \phi = \dfrac{C^* - C_\infty}{C_w - C_\infty}, Pr = \dfrac{\mu_b c_{bp}}{k_{Tb}}, Sc = \dfrac{D_0}{\upsilon_b}, P_0 = \dfrac{\partial P}{\partial x}, Da = \dfrac{k^*}{R_0^2} w, M = B_0 R_0 \sqrt{\dfrac{\sigma_{eb}}{\mu_b}} \end{array}\right\} \tag{13}$$

Simplifying equations (9) – (12), we shall now present the dimensionless equations for momentum, energy, and mass concentration as:

$$\frac{\partial w}{\partial t} = \left(\frac{\partial^2 w}{\partial r^2} + \frac{1}{r} \frac{\partial w}{\partial r} \right) + Gr\theta + Gc\phi - \frac{w}{Da} - M^2 w \tag{14}$$

$$Pr \frac{\partial \theta}{\partial t} = \frac{\partial^2 \theta}{\partial r^2} + \frac{1}{r} \frac{\partial \theta}{\partial r} \tag{15}$$

British Journal of Multidisciplinary and Advanced Studies5(4),14-32, 2024
Mathematics, Statistics, Quantitative and Operations Research,
Print ISSN: 2517-276X
Online ISSN: 2517-2778
https://bjmas.org/index.php/bjmas/index
Published by the European Centre for Research Training and Development UK

$$\frac{\partial \phi}{\partial t} = Sc\left(\frac{\partial^2 \phi}{\partial r^2} + \frac{1}{r}\frac{\partial \phi}{\partial r}\right) - Rd_2 Sc\phi + SrSc\left(\frac{\partial^2 \theta}{\partial r^2} + \frac{1}{r}\frac{\partial \theta}{\partial r}\right) \tag{16}$$

The corresponding boundary conditions are:

$$\left.\begin{array}{ll} w = 0, \theta = 1, \phi = 1, & \text{at } r = h \\ w \neq 0, \theta \neq 0, \phi \neq 0, & \text{at } r = 0 \end{array}\right\} \tag{17}$$

Perturbation Solution

We considered that the flow of blood in a channel is oscillatory pumping action of the heart, hence, the flow profiles are assumed to be in the form:

$$\left.\begin{array}{l} w = w_0 e^{\omega t} \\ \theta = \theta_0 e^{\omega t} \\ \phi = \phi_0 e^{\omega t} \end{array}\right\} \tag{18}$$

Applying equation (18) to equations (14) - (17), we have:

$$r\frac{d^2 w_0}{dr^2} + \frac{dw_0}{dr} - \lambda_1^2 r w_0 + rGr\theta_0 + Gcr\phi_0 = 0 \tag{19}$$

$$r\frac{d^2 \theta_0}{dr^2} + \frac{d\theta_0}{dr} - \lambda_2^2 r\theta_0 = 0 \tag{20}$$

$$r\frac{d^2 \phi_0}{dr^2} + \frac{d\phi_0}{dr} - \lambda_3^2 r\phi_0 + Sr\left(r\frac{d^2 \theta_0}{dr^2} + \frac{d\theta_0}{dr}\right) = 0 \tag{21}$$

$$\left.\begin{array}{ll} w_0 = 0, \theta_0 = e^{-\omega t}, \phi_0 = e^{-\omega t}, & \text{at } r = h \\ w_0 \neq 0, \theta_0 \neq 0, \theta_0 \neq 0, & \text{at } r = 0 \end{array}\right\} \tag{22}$$

where: $\lambda_1^2 = \frac{1}{Da} + M^2 + \omega, \lambda_2^2 = Pr\omega,$ and $\lambda_3^2 = \left(Rd + \frac{\omega}{Sc}\right)$

Method of Solution

The Laplace transform of the flow functions can be stated mathematically as:

British Journal of Multidisciplinary and Advanced Studies5(4),14-32, 2024
Mathematics, Statistics, Quantitative and Operations Research,
Print ISSN: 2517-276X
Online ISSN: 2517-2778
https://bjmas.org/index.php/bjmas/index
Published by the European Centre for Research Training and Development UK

$$\left.\begin{aligned} L\{w(r)\} &= w(s) = \int_0^\infty w(r)e^{-sr}dr \\ L\{\theta(r)\} &= \theta(s) = \int_0^\infty \theta(r)e^{-sr}dr \\ L\{\phi(r)\} &= \phi(s) = \int_0^\infty \phi(r)e^{-sr}dr \end{aligned}\right\} \quad (23)$$

Applying the method in equation (23) to dimensionless heat equation (20), we have;

$$\left(s^2 - Pr\omega\right)\frac{d\theta_0}{ds} = -s\theta_0(s) \quad (24)$$

where $\lambda_2^2 = Pr\omega$

Further simplification of equation (24), we have:

$$\theta_0(s) = \frac{A}{\sqrt{\left(s^2 - \lambda_2^2\right)}} \quad (25)$$

We know that: $\theta_0(r) = L^{-1}\{\theta_0(s)\}$, therefore, simplifying equation (25) gives;

$$\theta_0(r) = AI_0(\lambda_2 r) \quad (26)$$

where $I_0(\lambda_2 r)$ is the modified Bessel function of order zero.

Solving equation (26) using the boundary conditions in equation (22), we get the constant coefficient:

$$A = \frac{1}{I_0(\lambda_2 h)e^{\omega t}} \quad (27)$$

Putting equation (27) into equation (26), gives:

$$\theta_0(r) = \frac{I_0(\lambda_2 r)}{I_0(\lambda_2 h)e^{\omega t}} \quad (28)$$

where $I_0(\lambda_2 r) = \left(1 + \frac{\lambda_2^2 r^2}{4} + \frac{\lambda_2^4 r^4}{64} + \frac{\lambda_2^6 r^6}{2304} + \ldots\right)$ and $I_0(h\lambda_2) = \left(1 + \frac{h^2\lambda_2^2 r^2}{4} + \frac{h^4\lambda_2^4 r^4}{64} + \frac{h^6\lambda_2^6 r^6}{2304} + \ldots\right)$

Using equation (28), we can rewrite equation (18) as:

$$\theta(r) = \frac{1}{I_0(\lambda_2 h)}\left(1 + \frac{\lambda_2^2 r^2}{4} + \frac{\lambda_2^4 r^4}{64} + \frac{\lambda_2^6 r^6}{2304} + \ldots\right) \quad (29)$$

Substituting equation (28) into the mass concentration equation (21), we get:

$$\frac{d^2\phi_0}{dr^2}+\frac{1}{r}\frac{d\phi_0}{dr}-\lambda_3^2\phi_0=-\frac{\lambda_2^2 Sr}{I_0(\lambda_2 h)e^{\omega t}}\left(1+\frac{\lambda_2^2 r^2}{4}+\frac{\lambda_2^4 r^4}{64}\right) \tag{30}$$

Presenting equation (30) with particular term, we have:

$$r\frac{d^2\phi_{0p}}{dr^2}+\frac{d\phi_{0p}}{dr}-\lambda_3^2 r\phi_{0p}=-\frac{\lambda_2^2 Sr}{I_0(\lambda_2 h)e^{\omega t}}\left(r+\frac{\lambda_2^2 r^3}{4}+\frac{\lambda_2^4 r^5}{64}\right) \tag{31}$$

The particular solution of equation (31) can be presented as:

$$\phi_{0p}=A_0+A_1 r+A_2 r^2+A_3 r^3+A_4 r^4+A_5 r^5 \tag{32}$$

Solving equation (31), we have:

$$\left.\begin{aligned} A_0&=\frac{Sr}{I_0(\lambda_2 h)e^{\omega t}}\left\{\frac{\lambda_2^2}{\lambda_3^2}+\frac{\lambda_2^4}{\lambda_3^4}+\frac{\lambda_2^6}{\lambda_3^6}\right\},\ A_1=0,\\ A_2&=\frac{Sr}{4I_0(\lambda_2 h)e^{\omega t}}\left\{\frac{\lambda_2^4}{\lambda_3^2}+\frac{\lambda_2^6}{\lambda_3^4}\right\},A_3=0,\\ A_4&=\frac{\lambda_2^6}{64\lambda_3^2}\frac{Sr}{I_0(\lambda_2 h)e^{\omega t}},A_5=0, \end{aligned}\right\} \tag{33}$$

Substituting equation (33) into equation (32), we have:

$$\phi_{0p}=\frac{Sr}{I_0(\lambda_2 h)e^{\omega t}}\left\{\frac{\lambda_2^2}{\lambda_3^2}+\frac{\lambda_2^4}{\lambda_3^4}+\frac{\lambda_2^6}{\lambda_3^6}\right\}+\frac{Sr}{4I_0(\lambda_2 h)e^{\omega t}}\left\{\frac{\lambda_2^4}{\lambda_3^2}+\frac{\lambda_2^6}{\lambda_3^4}\right\}r^2+\frac{\lambda_2^6}{64\lambda_3^2}\frac{Sr}{I_0(\lambda_2 h)e^{\omega t}}r^4 \tag{34}$$

The homogeneous solution of equation (31) is:

$$\phi_{0h}=c_2 I_0(\lambda_3 r) \tag{35}$$

The general solution of equation (31) is the sum of the homogeneous and particular solutions:

$$\phi_0=c_2 I_0(\lambda_3 r)+\frac{Sr}{I_0(\lambda_2 h)e^{\omega t}}\left\{\frac{\lambda_2^2}{\lambda_3^2}+\frac{\lambda_2^4}{\lambda_3^4}+\frac{\lambda_2^6}{\lambda_3^6}\right\}+\frac{Sr}{4I_0(\lambda_2 h)e^{\omega t}}\left\{\frac{\lambda_2^4}{\lambda_3^2}+\frac{\lambda_2^6}{\lambda_3^4}\right\}r^2+\frac{\lambda_2^6}{64\lambda_3^2}\frac{Sr}{I_0(\lambda_2 h)e^{\omega t}}r^4 \tag{36}$$

Using the boundary conditions in equation (22), we get:

$$c_2=\left\{\begin{aligned}&\frac{e^{-\omega t}}{I_0(\lambda_3 h)}-\frac{Sr}{I_0(\lambda_2 h)I_0(\lambda_3 h)e^{\omega t}}\left\{\frac{\lambda_2^2}{\lambda_3^2}+\frac{\lambda_2^4}{\lambda_3^4}+\frac{\lambda_2^6}{\lambda_3^6}\right\}-\frac{Sr}{4I_0(\lambda_2 h)I_0(\lambda_3 h)e^{\omega t}}\left\{\frac{\lambda_2^4}{\lambda_3^2}+\frac{\lambda_2^6}{\lambda_3^4}\right\}h^2\\&-\frac{\lambda_2^6}{64\lambda_3^2}\frac{Sr}{I_0(\lambda_2 h)I_0(\lambda_3 h)e^{\omega t}}h^4\end{aligned}\right\} \tag{37}$$

Therefore, equation (36) becomes:

$$\phi_0 = c_2 I_0(\lambda_3 r) + A_0 + A_1 r^2 + A_2 r^4 \tag{38}$$

where

$$A = \frac{Gr}{I_0(\lambda_2 h)}, A_0 = \frac{SrGc}{I_0(\lambda_2 h)e^{\omega t}}\left\{\frac{\lambda_2^2}{\lambda_3^2} + \frac{\lambda_2^4}{\lambda_3^4} + \frac{\lambda_2^6}{\lambda_3^6}\right\}, A_1 = \frac{SrGc}{4I_0(\lambda_2 h)e^{\omega t}}\left\{\frac{\lambda_2^4}{\lambda_3^2} + \frac{\lambda_2^6}{\lambda_3^4}\right\}, A_2 = \frac{\lambda_2^6}{64\lambda_3^2}\frac{SrGc}{I_0(\lambda_2 h)e^{\omega t}}$$

To solve for the velocity profile, let's recall equation (19):

$$\frac{d^2 w_0}{dr^2} + \frac{1}{r}\frac{dw_0}{dr} - \lambda_1^2 w_0 = -Gr\theta_0 - Gc\phi_0 \tag{39}$$

Substituting equation (38) and (28) into equation (39), we have the particular equation as:

$$\frac{d^2 w_{0p}}{dr^2} + \frac{1}{r}\frac{dw_{0p}}{dr} - \lambda_1^2 w_{0p} = -A_0 - AI_0(\lambda_2 r) - c_2 I_0(\lambda_3 r) - A_1 r^2 - A_2 r^4 \tag{40}$$

The solution of equation (40) can be represented as:

$$w_{0p} = B_0 + B_1 I_0(\lambda_2 r) + B_2 I_0(\lambda_3 r) + B_3 r^2 + B_4 r^4 \tag{41}$$

Solving equation (41) we get:

$$B_0 = \frac{A_0}{\lambda_1^2} + \left(\frac{2A_1}{\lambda_1^4} + \frac{18A_2}{\lambda_1^6}\right), B_1 = \frac{A}{\lambda_1^2}, B_2 = \frac{c_2}{\lambda_1^2}, B_3 = \left(\frac{A_1}{\lambda_1^2} + \frac{9A_2}{\lambda_1^4}\right), B_4 = \frac{A_2}{\lambda_1^2} \tag{42}$$

Recall the homogenous part of equation (39):

$$r\frac{d^2 w_{0h}}{dr^2} + \frac{dw_{0h}}{dr} - \lambda_1^2 r w_{0h} = 0 \tag{43}$$

Solving equation (43), we have:

$$w_{0h}(r) = c_3 I_0(\lambda_1 r) \tag{44}$$

Therefore, the general solution is:

$$w_0(r) = c_3 I_0(\lambda_1 r) + B_0 + B_1 I_0(\lambda_2 r) + B_2 I_0(\lambda_3 r) + B_3 r^2 + B_4 r^4 \tag{45}$$

Therefore, equation (12) becomes:

$$w(r,t) = \left(c_3 I_0(\lambda_1 r) + B_0 + B_1 I_0(\lambda_2 r) + B_2 I_0(\lambda_3 r) + B_3 r^2 + B_4 r^4\right)e^{\omega t} \tag{46}$$

where:

British Journal of Multidisciplinary and Advanced Studies5(4),14-32, 2024
Mathematics, Statistics, Quantitative and Operations Research,
Print ISSN: 2517-276X
Online ISSN: 2517-2778
https://bjmas.org/index.php/bjmas/index
Published by the European Centre for Research Training and Development UK

$$A=\frac{Gr}{I_0\left(\lambda_2 h\right)}, A_0=\frac{SrGc}{I_0\left(\lambda_2 h\right)e^{\omega t}}\left\{\frac{\lambda_2^2}{\lambda_3^2}+\frac{\lambda_2^4}{\lambda_3^4}+\frac{\lambda_2^6}{\lambda_3^6}\right\}, A_1=\frac{SrGc}{4I_0\left(\lambda_2 h\right)e^{\omega t}}\left\{\frac{\lambda_2^4}{\lambda_3^2}+\frac{\lambda_2^6}{\lambda_3^4}\right\}, A_2=\frac{\lambda_2^6}{64\lambda_3^2}\frac{SrGc}{I_0\left(\lambda_2 h\right)e^{\omega t}}$$

$$c_2=\left\{\begin{array}{l}\dfrac{e^{-\omega t}}{I_0\left(\lambda_3 h\right)}-\dfrac{Sr}{I_0\left(\lambda_2 h\right)I_0\left(\lambda_3 h\right)e^{\omega t}}\left\{\dfrac{\lambda_2^2}{\lambda_3^2}+\dfrac{\lambda_2^4}{\lambda_3^4}+\dfrac{\lambda_2^6}{\lambda_3^6}\right\}-\dfrac{Sr}{4I_0\left(\lambda_2 h\right)I_0\left(\lambda_3 h\right)e^{\omega t}}\left\{\dfrac{\lambda_2^4}{\lambda_3^2}+\dfrac{\lambda_2^6}{\lambda_3^4}\right\}h^2 \\ -\dfrac{\lambda_2^6}{64\lambda_3^2}\dfrac{Sr}{I_0\left(\lambda_2 h\right)I_0\left(\lambda_3 h\right)e^{\omega t}}h^4\end{array}\right\}$$

$$B_0=\frac{A_0}{\lambda_1^2}+\left(\frac{2A_1}{\lambda_1^4}+\frac{18A_2}{\lambda_1^6}\right), B_1=\frac{A}{\lambda_1^2}, B_2=\frac{c_2}{\lambda_1^2}, B_3=\left(\frac{A_1}{\lambda_1^2}+\frac{9A_2}{\lambda_1^4}\right), B_4=\frac{A_2}{\lambda_1^2}$$

$$c_3=-\frac{B_0}{I_0\left(\lambda_1 h\right)}-B_1\frac{I_0\left(\lambda_2 h\right)}{I_0\left(\lambda_1 h\right)}-B_2\frac{I_0\left(\lambda_3 h\right)}{I_0\left(\lambda_1 h\right)}-\frac{B_3 h^2}{I_0\left(\lambda_1 h\right)}-\frac{B_4 h^4}{I_0\left(\lambda_1 h\right)}$$

PRESENTATION OF RESULTS

Wolfram Mathematica version 12 was used to run a numerical simulation. We varied the parameters within a specific range to investigate their impact on the flow profile. The results are divided into three sections: the first is for the blood temperature profile, the second shows the plots for mass concentration profiles, and the third focuses on the plots for the blood velocity profile under various values of the relevant parameters. However, the parameter data used in the simulation were obtained from Bunonyo *et al.* (2021), Bunonyo and Ebiwareme (2022), and Bunonyo and Amos (2022), respectively.

British Journal of Multidisciplinary and Advanced Studies5(4),14-32, 2024
Mathematics, Statistics, Quantitative and Operations Research,
Print ISSN: 2517-276X
Online ISSN: 2517-2778
https://bjmas.org/index.php/bjmas/index
Published by the European Centre for Research Training and Development UK

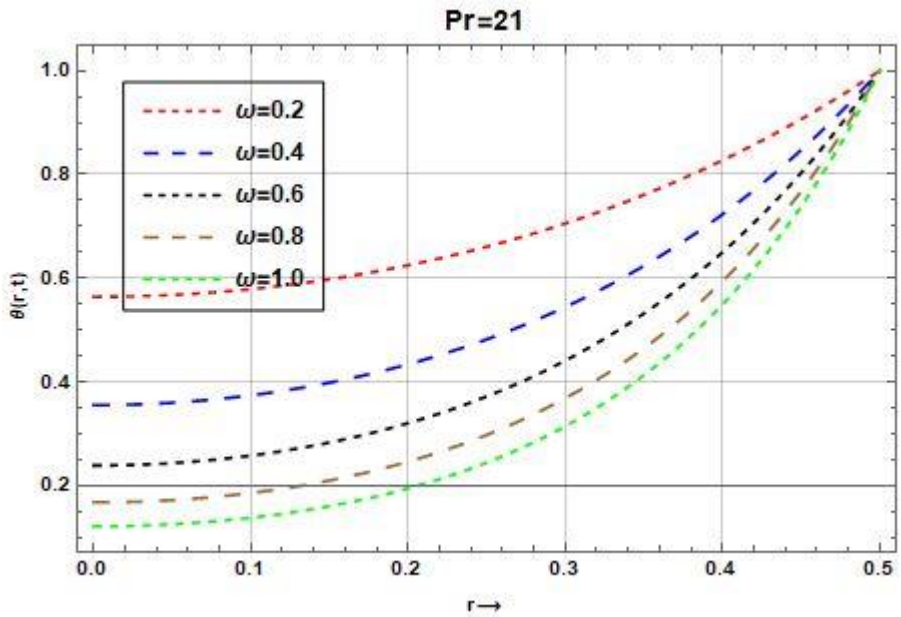

Figure 1 The effect of oscillation on the fluid temperature

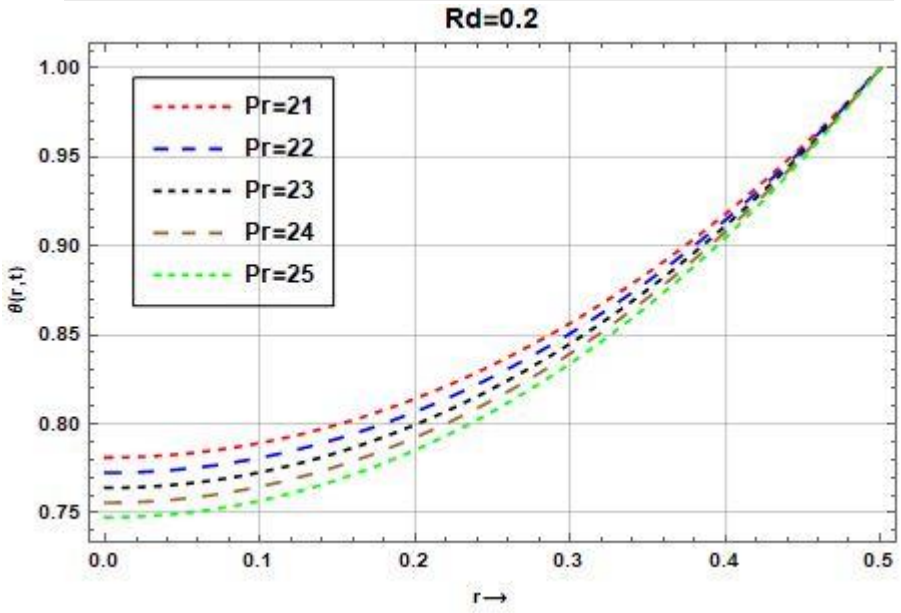

Figure 2 The effect of Prandtl number on the fluid temperature

British Journal of Multidisciplinary and Advanced Studies5(4),14-32, 2024
Mathematics, Statistics, Quantitative and Operations Research,
Print ISSN: 2517-276X
Online ISSN: 2517-2778
https://bjmas.org/index.php/bjmas/index
Published by the European Centre for Research Training and Development UK

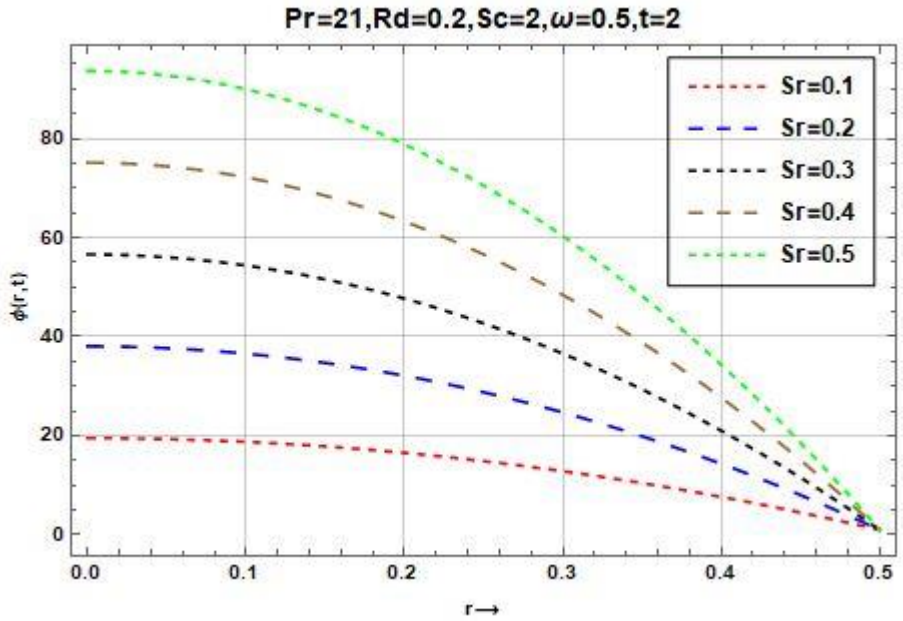

Figure 3 The effect of Soret number on mass concentration

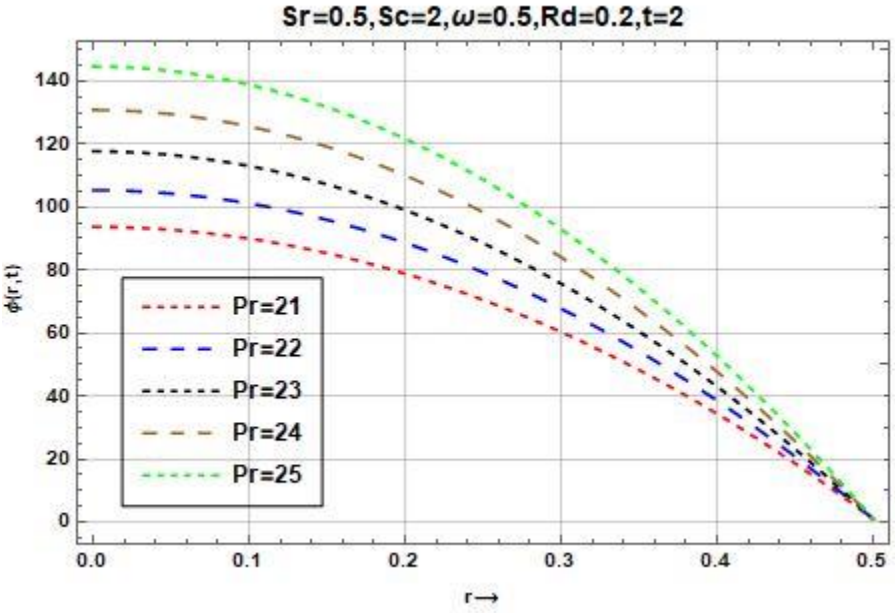

Figure 4 The effect of Prandtl number on mass concentration

British Journal of Multidisciplinary and Advanced Studies5(4),14-32, 2024
Mathematics, Statistics, Quantitative and Operations Research,
Print ISSN: 2517-276X
Online ISSN: 2517-2778
https://bjmas.org/index.php/bjmas/index
Published by the European Centre for Research Training and Development UK

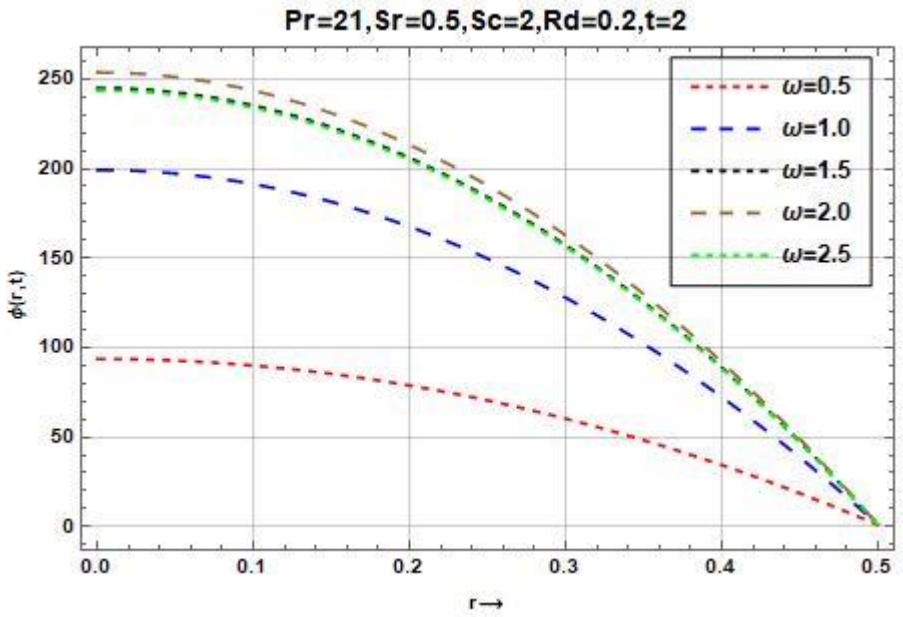

Figure 5 The effect of oscillatory number on mass concentration

British Journal of Multidisciplinary and Advanced Studies5(4),14-32, 2024
Mathematics, Statistics, Quantitative and Operations Research,
Print ISSN: 2517-276X
Online ISSN: 2517-2778
https://bjmas.org/index.php/bjmas/index
Published by the European Centre for Research Training and Development UK

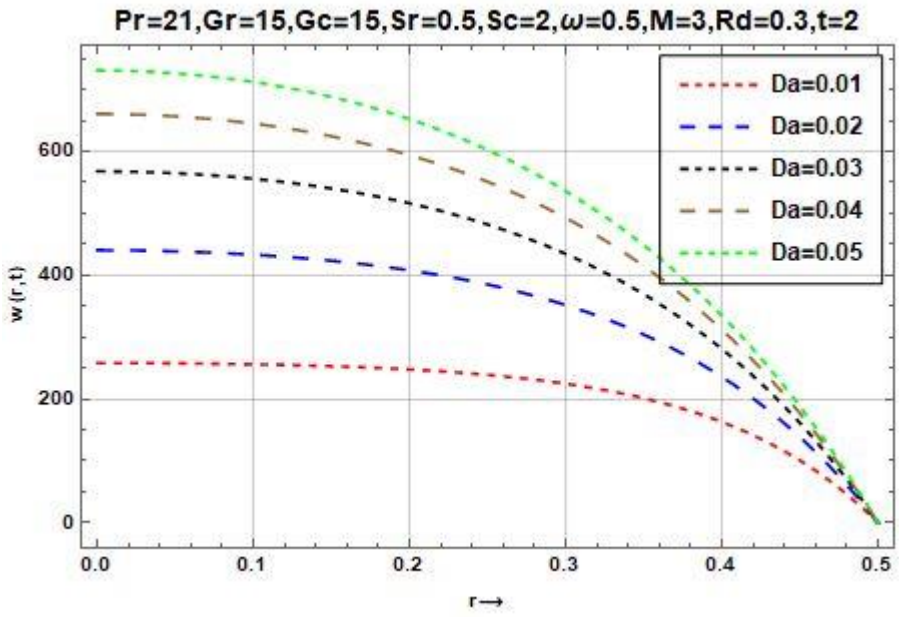

Figure 6 The effect of Darcy number on the fluid velocity

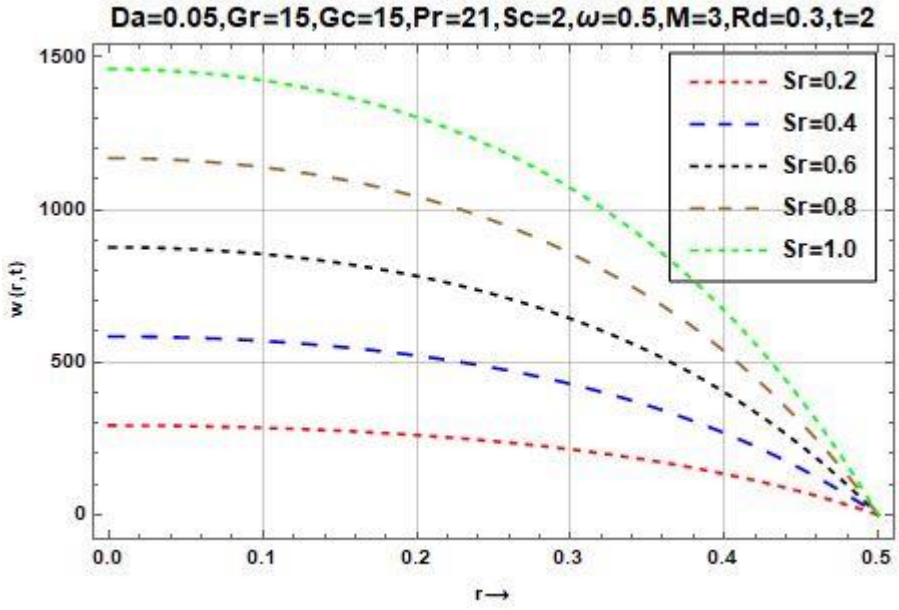

Figure 7 The effect of Soret number on the fluid velocity

British Journal of Multidisciplinary and Advanced Studies5(4),14-32, 2024
Mathematics, Statistics, Quantitative and Operations Research,
Print ISSN: 2517-276X
Online ISSN: 2517-2778
https://bjmas.org/index.php/bjmas/index
Published by the European Centre for Research Training and Development UK

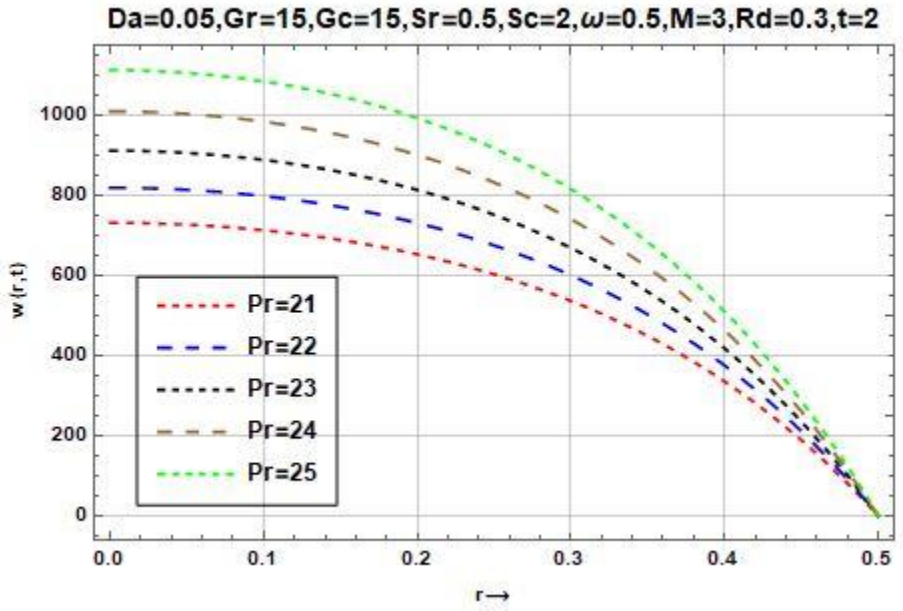

Figure 8 The effect of Prandtl number on the fluid velocity

DISCUSSION OF RESULTS

It's observed in figure 1 that the temperature profile increases along the boundary for the Prandtl number $Pr = 21$ and the oscillatory frequency at $\omega = 0.2$. However, the profile showed a decrease in temperature profile for the increasing values of the oscillatory frequency $\omega = 0.2, 0.4, 0.6, 0.8, 1.0$ before converging to 1 as the boundary layer attains its peak of 0.5. We can also observed in figure 2 that the temperature profile increases along the boundary for the chemical reaction parameter $Rd = 0.2$ and the Prandtl number at $Pr = 21$. However, the profile indicates a decrease in temperature profile though much slower than that of increasing oscillatory frequency, for the increasing values of the Prandtl number $Pr = 21, 22, 23, 24, 25$ before converging to 1 as the boundary layer attains its peak of 0.5. Figure 3 showed that the mass concentration profile decreases along the boundary layer where other pertinent parameters are considered as $Rd = 0.2, Sc = 0.2, \omega = 0.5, , Pr = 21, t = 2$ and the Soret number at $Sr = 0.1$. However, it can be seen in the figure that the mass concentration continuously decreased for different rate of increase of the Soret number $Sr = 0.2, 0.4, 0.6, 0.8, 1.0$ before converging to 0 as the boundary layer attains its maximum value of 0.5. Figure 4 showed that the mass concentration profile increases along the boundary layer thickness where other pertinent parameters are considered as $Rd = 0.2, Sc = 0.2, \omega = 0.5, Sr = 0.1, t = 2$ and the Prandtl number at $Pr = 21$. The

observation in the figure is of the view that the mass concentration slowly increases for different values of the Prandtl number $Pr = 21, 22, 23, 24, 25$ before converging to 0 as the boundary layer attains its maximum value of 0.5.

Figure 5 showed that the mass concentration profile increases along the boundary layer thickness where other pertinent parameters are considered as $Rd = 0.2, Sc = 0.2, Pr = 21, Sr = 0.5, t = 2$ and the oscillatory frequency of $\omega = 0.5$. The observation indicates that the mass concentration slowly increases for different values of the oscillatory frequency $\omega = 0.5, 1.0, 1.5, 2.0, 2.5$ before converging to 0 as the boundary layer thickness grows to 0.5.

Figure 6 indicates the effect of Darcy number on blood velocity profile, and it can be seen that the velocity decreases along the boundary layer thickness increases where other pertinent parameters are considered as $Rd = 0.3, Sc = 2, Sr = 0.2, M = 3, Gr = 15, Gc = 15, Pr = 21, t = 2$ and the Darcy number of $Da = 0.01$. However, the velocity profile increases for different values of the Darcy number $Da = 0.01, 0.02, 0.03, 0.04, 0.05$ before decreasing to $w = 0$ as the boundary layer thickness grows to $r = 0.5 < \infty$.

Figure 7 showed the effect of Soret number on blood velocity profile, and it can be seen that the velocity decreases along the boundary layer thickness where other pertinent parameters are considered as $Rd = 0.3, Sc = 2, Pr = 21, M = 3, Gr = 15, Gc = 15, Da = 0.05, t = 2$ and the Soret number of $Sr = 0.2$. However, the velocity profile increases for different values of the Soret number $Sr = 0.2, 0.4, 0.6, 0.8, 1.0$ before decreasing to $w = 0$ as the boundary layer thickness grows to $r = 0.5 < \infty$.

Figure 8 showed the effect of Prandtl number on blood velocity profile, and it can be seen that the velocity decreases along the boundary layer thickness where other pertinent parameters are considered as $Rd = 0.3, Sc = 2, Sr = 0.5, M = 3, Gr = 15, Gc = 15, Da = 0.05, t = 2$ and the Prandtl number of $Pr = 21$. However, the velocity profile increases for different values of the Prandtl number $Pr = 21, 22, 23, 24, 25$ before decreasing to $w = 0$ as the boundary layer thickness grow to $r = 0.5 < \infty$.

CONCLUSION

Following the mathematical formulation to investigate the thermosolutal effect on blood flow through a micro-channel in the presence of a magnetic field, the provision of an analytical solution, and a numerical simulation using Wolfram Mathematica, version 12, we can conclude by discussing our results as follows:

1. The temperature profile increases as the boundary layer thickness increase for the Prandtl number $Pr = 21$ and the oscillatory frequency at $\omega = 0.2$. But decreases as the oscillatory frequency increases at the fixed Prandtl number.
2. The temperature profile increases as the boundary layer thickness increase for the chemical reaction parameter at $Rd = 0.2$ and the Prandtl number of $Pr = 21$. But decreases as the Prandtl number of $Pr = 21, 22, 23, 24, 25$.
3. The mass concentration profile decreases along the boundary layer where other pertinent parameters are considered as $Rd = 0.2, Sc = 0.2, \omega = 0.5, , Pr = 21, t = 2$ and the Soret number at $Sr = 0.1$. And mass concentration continuously decreased for increase of the Soret number $Sr = 0.2, 0.4, 0.6, 0.8, 1.0$
4. The mass concentration profile increases along the boundary layer thickness where other pertinent parameters are considered as $Rd = 0.2, Sc = 0.2, \omega = 0.5, Sr = 0.1, t = 2$ and the Prandtl number at $Pr = 21$.
5. The mass concentration profile increases along the boundary layer thickness where other pertinent parameters are considered as $Rd = 0.2, Sc = 0.2, Pr = 21, Sr = 0.5, t = 2$ and the oscillatory frequency of $\omega = 0.5$.
6. The effect of Darcy number on blood velocity profile and it can be seen that the velocity decreases along the boundary layer thickness increase where other pertinent parameters are considered as $Rd = 0.3, Sc = 2, Sr = 0.2, M = 3, Gr = 15, Gc = 15, Pr = 21, t = 2$ and the Darcy number of $Da = 0.01$.
7. The effect of Soret number on blood velocity profile and it can be seen that the velocity decreases along the boundary layer thickness where other pertinent parameters are considered as $Rd = 0.3, Sc = 2, Pr = 21, M = 3, Gr = 15, Gc = 15, Da = 0.05, t = 2$ and the Soret number of $Sr = 0.2$.
8. The effect of Prandtl number on blood velocity profile and it can be seen that the velocity decreases along the boundary layer thickness where other pertinent parameters are considered as $Rd = 0.3, Sc = 2, Sr = 0.5, M = 3, Gr = 15, Gc = 15, Da = 0.05, t = 2$ and the Prandtl number of $Pr = 21$. However, the velocity profile increases for different values of the Prandtl number $Pr = 21, 22, 23, 24, 25$

Conflict of Interest

The authors declare no conflict of interest

References

Athani, A., Ghazali, N. N. N., Badruddin, I. A., Kamangar, S., Anqi, A. E., &Algahtani, A. (2022). Investigation of two-way fluid-structure interaction of blood flow in a patient-specific left coronary artery. *Bio-Medical Materials and Engineering*, *33*(1), 13-30

Bunonyo, K. W., & Ebiwareme, L. (2022). A low Prandtl number haemodynamic oscillatory flow through a cylindrical channel using the Power Series Method. European Journal of Applied Physics, 4(3), 56-65.

Bunonyo, K. W., Amos, E., & Eli, I. C. (2018). Unsteady oscillatory couette flow between vertical parallel plates with constant radiative heat flux. *Asian Research Journal of Mathematics*, *11*(2), 1-11.

Bunonyo, K. W., & Amos, E. (2020). Lipid concentration effect on blood flow through an inclined arterial channel with magnetic field. *Mathematical modelling and Applications*, *5*(3), 129.

Bunonyo, K. W., Amos, E., & Nwaigwe, C. (2021). Modeling the treatment effect on LDL-C and atherosclerotic blood flow through microchannel with heat and magnetic field. *International Journal of Mathematics Trends and Technology-IJMTT*, *67*.

Bunonyo, K. W., & Amos, E. (2022). Convective Flow of Blood through a Constricted Cylinder and the Effect of Cholesterol Growth Rate on the Motion in the Presence of a Magnetic Field. *African Scientific Reports*, 174-187.

Ebiwareme, L., & Bunonyo, K. W. (2024). Chemical Reaction and Nonlinear Rosseland Approximation Effects On Double-Diffusive MHD Sisko Nanofluid Flow Over a Nonlinear Stretching Sheet in A Porous Medium with Concentration-Dependent Internal Heat Source. British Journal of Multidisciplinary and Advanced Studies, 5(1), 1-20.

Fahim, M., Sajid, M., & Ali, N. (2024). Pulsatile pressure-driven non-Newtonian blood flow through a porous stenotic artery: A computational analysis. Numerical Heat Transfer, Part A: Applications, 1-21.

Gul, T., Nasir, S., Berrouk, A. S., Raizah, Z., Alghamdi, W., Ali, I., & Bariq, A. (2023). Simulation of the water-based hybrid nanofluids flow through a porous cavity for the applications of the heat transfer. *Scientific Reports*, *13*(1), 7009.

Hosseinzadeh, S., Hosseinzadeh, K., Hasibi, A., & Ganji, D. D. (2022). Hydrothermal analysis on non-Newtonian nanofluid flow of blood through porous vessels. Proceedings of the Institution of Mechanical Engineers, Part E: Journal of Process Mechanical Engineering, 236(4), 1604-1615.

Kubugha, B. W., & Amos, E. (2022). Mathematical Modeling of LDL-C and Blood Flow through an Inclined Channel with Heat in the Presence of Magnetic Field. Trends in Sciences, 19(16), 5693-5693.

Hanvey, R. R., & Bunonyo, K. W. (2022). Effect of treatment parameter on oscillatory flow of blood through an atherosclerotic artery with heat transfer. *Journal of the Nigerian Society of Physical Sciences*, 682-682.

Kumawat, C., Sharma, B. K., &Mekheimer, K. S. (2021). Mathematical analysis of two-phase blood flow through a stenosed curved artery with hematocrit and temperature dependent viscosity. Physica Scripta, 96(12), 125277.

Mamun, K., Funazaki, K., Akter, S., & Akhter, M. N. (2020). The effect of magnetic field on blood flow through stenotic artery-a review on bio-magnetic fluid dynamics. Series on Biomechanics, 34(1), 20-30.

Priyadharsini, M. (2023). Mathematical modelling and analysis of thermoregulation effects on blood viscosity under magnetic effects and thermal radiation in a permeable stretching capillary. Journal of Thermal Biology, 111, 103398.

Selvi, R. T., Ponalagusamy, R., & Padma, R. (2021). Influence of electromagnetic field and thermal radiation on pulsatile blood flow with nanoparticles in a constricted porous artery. International Journal of Applied and Computational Mathematics, 7, 1-25.

Shah, N. A., Al-Zubaidi, A., & Saleem, S. (2021). Study of Magnetohydrodynamic Pulsatile Blood Flow through an Inclined Porous Cylindrical Tube with Generalized Time-Nonlocal Shear Stress. *Advances in Mathematical Physics*, *2021*(1), 5546701.

Sharma, B. K., Gandhi, R., Abbas, T., & Bhatti, M. M. (2023). Magnetohydrodynamics hemodynamics hybrid nanofluid flow through inclined stenotic artery. Applied Mathematics and Mechanics, 44(3), 459-476.

Verma, N., & Parihar, R. S. (2010). Mathematical model of blood flow through a tapered artery with mild stenosis and hematocrit. J. Mod. Math. Stat, 4(1), 38-43.

Yadav, P. K., & Roshan, M. (2024). Mathematical modeling of blood flow in an annulus porous region between two coaxial deformable tubes: An advancement to peristaltic endoscope. *Chinese Journal of Physics*, *88*, 89-109.

Yusuf, S., Lonn, E., Pais, P., Bosch, J., López-Jaramillo, P., Zhu, J. ... & Parkhomenko, A. (2016). Blood-pressure and cholesterol lowering in persons without cardiovascular disease. New England Journal of Medicine, 374(21), 2032-2043.